

# PROCEEDINGS OF SPIE

[SPIDigitalLibrary.org/conference-proceedings-of-spie](https://SPIDigitalLibrary.org/conference-proceedings-of-spie)

## Differences in ice and water LWIR spectral polarimetry at room temperature

Jaclyn John, Jeremy Parkinson, Meredith Kupinski

Jaclyn A. John, Jeremy C. Parkinson, Meredith K. Kupinski, "Differences in ice and water LWIR spectral polarimetry at room temperature," Proc. SPIE 12690, Polarization Science and Remote Sensing XI, 126900I (3 October 2023); doi: 10.1117/12.2678064

**SPIE.**

Event: SPIE Optical Engineering + Applications, 2023, San Diego, California, United States

# Differences in Ice and Water LWIR Spectral Polarimetry at Room Temperature

Jaclyn A. John<sup>a</sup>, Jeremy C. Parkinson<sup>a</sup>, and Meredith K. Kupinski<sup>a</sup>

<sup>a</sup>University of Arizona, 1600 E. University Blvd., Tucson, USA

## ABSTRACT

The University of Arizona Polarization Lab developed an Infrared Channeled Spectro-Polarimeter (IRCSP) to measure linear Stokes parameters with  $1K$  polarimetric accuracy and  $1\mu\text{m}$  average spectral resolution between  $8\text{-}11\mu\text{m}$ .<sup>1-3</sup> Emissivity and refractive index in this spectral band are known to depend upon water's kinetic temperature and thermodynamic phase. In this work, the theoretical thermodynamic phase discrimination capabilities of spectral Long-Wave-Infrared (LWIR) polarimetry are demonstrated with IRCSP. In a room temperature laboratory environment, IRCSP measurements of melting ice are shown to depend on the view angle, wavelength, and thermodynamic phase. As the solid ice melted for 10 minutes, IRCSP measured a constant brightness temperature of  $276K$  between the time-lapsed samples. The difference in the degree of linear polarization (DoLP) between solid and melted ice was 7% on average and peaked at 13% in the  $9.5\text{-}10.5\mu\text{m}$  waveband. This observation is an example of enhanced sensitivity to thermodynamic phase change using LWIR polarimetry.

## 1. INTRODUCTION

### 1.1 Ice-Water Discrimination

Many environmental science applications require discrimination between the thermodynamic phases of water. Earth's cryosphere is changing rapidly, and melting sea ice can affect large-scale ocean circulation patterns that change the global environment. IceSAT-2, launched in 2018 as part of NASA's Earth Observing System, uses a photon-counting laser altimeter to measure melting ice sheets and determine the elevation of glaciers.<sup>4</sup> Differentiating between ice and water is relevant to the IceSAT-2 mission because both the height of the ice surface and the height of the sea surface need to be measured to calculate the elevation of ice surfaces protruding from the water.<sup>5</sup> Ice and water have significantly different emission and backscattering properties in the microwave region. Microwave radiometers are currently the primary instrument used for the estimation of sea ice concentration, the detection of areas covered in multi-year ice, and the discrimination between water surfaces and different types of ice in the polar regions.<sup>6,7</sup> Ice and water discrimination in clouds is another region of interest. Whether a cloud is made from water droplets, ice crystals, or a mixture of both influences its radiative impact on atmospheric processes.<sup>8,9</sup> Both polarized Micro Pulse Lidar measurements and NIR spectro-radiometers have been previously demonstrated as a method for distinguishing the thermodynamic phase of clouds.<sup>10,11</sup> Finally, ice-water discrimination is also important for safety mitigation, such as in the application of detecting ice build-up on aircraft.<sup>12</sup> In this work, spectral LWIR polarimetric measurements are performed in an uncontrolled room temperature laboratory environment to investigate ice-water discrimination capabilities.

### 1.2 Optical Properties of Water

Published values of the index of refraction differences in the LWIR wavebands for ice and water are shown in Figure 1.<sup>13</sup> Many liquids, such as water, are composed of molecules that have permanent electric dipole moments. In the absence of an external field the ensemble dipole orientation is randomly distributed. However, in the presence of an external field, the water absorbs radiation to reorient the molecules. The dipoles attempt to align to the external field and an opposing restoring force is also created. The process in which the dipoles "relax" to equilibrium is called Debye relaxation.<sup>14</sup> This relaxation time is highly temperature-dependent.<sup>15</sup> In the phase transition from liquid to solid water the electric dipoles in the liquid lose their orientational mobility and are unable to reorient themselves in the solid. Therefore, as the water's kinetic temperature decreases, Debye relaxation vanishes. Dipole relaxation is the source of the high absorption of water in microwave and infrared regions. Notable spectral absorption differences between solid and liquid water in the LWIR are due

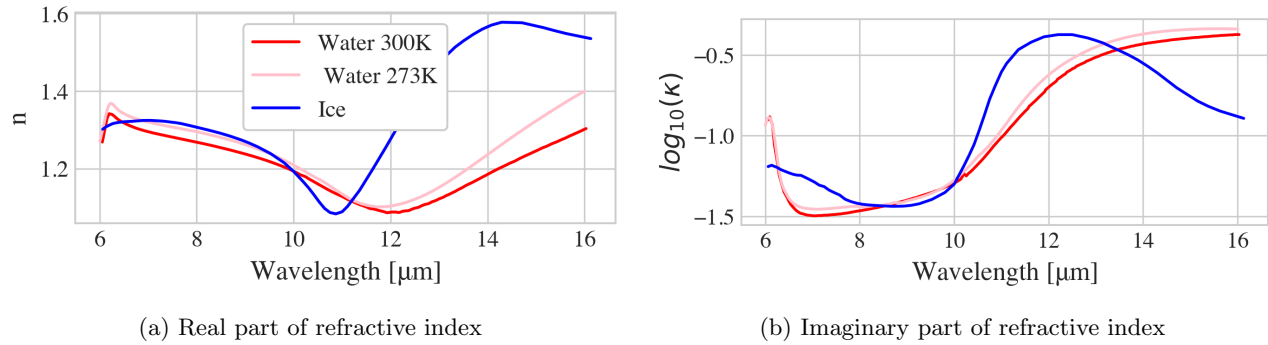


Figure 1: Refractive index  $\tilde{n} = n + i\kappa$  of ice, 273K water, and 300K water in the LWIR band.<sup>13,17</sup> The refractive index of water depends on the kinetic temperature. The real and imaginary part of ice and water at 300K intersect at approximately  $10.0\mu\text{m}$  and at a smaller wavelength for the 273K water. In (a), regions of anomalous dispersion where  $n$  is increasing with wavelength occur around  $12.0\mu\text{m}$  as a resonant vibrational frequency of ice. In (b), the peak absorption wavelengths include  $6.05\mu\text{m}$  in liquid water which shifts to  $12.0\mu\text{m}$  for ice.

to Debye relaxation.<sup>14</sup> Molecular vibrations are another dominant mechanism for absorption in the LWIR. The fundamental vibration modes of the  $H_2O$  molecule occur at different frequencies which correspond to the peak absorption wavelengths in ice and water. Ice and water have different vibrational frequencies because, as water freezes and molecules are locked into a lattice structure, the vibrations slow down. Therefore, ice will have lower resonant vibrational frequencies and absorption peaks at longer wavelengths.

Regions of high absorption, in the vicinity of the resonant vibrational frequencies, are where anomalous dispersion is observed. Anomalous dispersion occurs when the real part of the refractive index increases with wavelength. In Figure 1a, there is a region of anomalous dispersion in ice centered around the peak absorption wavelength  $12.0\mu\text{m}$  where  $n$  is increasing as wavelength increases. Anomalous dispersion is expected to occur in different spectral regions for ice and water.<sup>14,16</sup> In liquid water, there is a peak absorption wavelength at  $6.05\mu\text{m}$ . The peak absorption wavelengths of  $6.05\mu\text{m}$  and  $12.0\mu\text{m}$  for water and ice respectively are shown in Figure 1b.

### 1.3 Polarized Emissivity

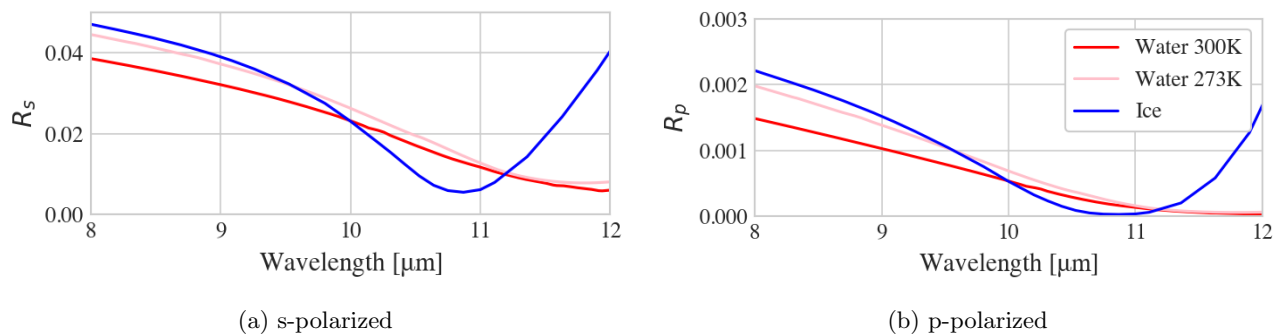


Figure 2: LWIR spectral dependence of Fresnel reflection at  $45^\circ$  view angle. In (a) s-polarized and in (b) p-polarized. The scale of  $R_p$  is an order of magnitude less than  $R_s$ . Ice is more reflective than water over most of the LWIR waveband with the exception of a dip in  $R_s$  at  $10.8\mu\text{m}$ .

The LWIR spectral dependence of Fresnel reflection coefficients for ice, water at 300K, and water at 273K are shown in Figure 2 for a  $45^\circ$  view angle. The polarization of light describes the direction of oscillation of the transverse electric field. Light being reflected or transmitted through a material becomes polarized as a result of

Fresnel interactions at the optical interfaces. Light polarized perpendicular to the plane of incidence is referred to as s-polarization, while light polarized parallel to the plane of incidence is p-polarization. The Fresnel intensity coefficients represent the flux in the reflected and transmitted beams relative to the flux of incident light. The reflection intensity coefficients for the s- and p-polarized light depend on the incident and transmitted refractive indices, view angle, and the transmitted angle.<sup>14,18</sup>

In the LWIR waveband, thermal radiation becomes polarized from both reflection and emission.<sup>19,20</sup> Kirchoff's law expresses that at thermal equilibrium, the emissivity is equal to the absorption because all absorbed radiation is re-radiated. For energy to be conserved in light-matter interactions, reflectivity, transmittance, and absorption sum to unity.<sup>19</sup> For an opaque medium, the transmission is negligible. Therefore, water, which is opaque in the LWIR, has a polarized emissivity that can be described as  $e_{s,p} = 1 - R_{s,p}$ . The emissivity is thereby dependent on the refractive index of the material, as well as the incidence angle. The polarization difference (PD) is defined as  $PD = \frac{e_s - e_p}{e_s + e_p}$ .<sup>21</sup> Figure 3 shows how the emissivity and therefore the PD of water changes as a function of wavelength, viewing angle, and the water's thermodynamic phase and kinetic temperature. There are a few notable wavelengths where the emissivity and polarization for ice and water intersect one another. The emissivity and polarization of ice and water at 300K intersect at approximately 10.0 $\mu$ m and 11.2 $\mu$ m. The emissivity and polarization of ice and water at 273K intersect at approximately 9.5 $\mu$ m and 11.2 $\mu$ m. Figures 3c and 3d show notable differences in the spectrally dependent polarization magnitudes of ice and water at 273K. At the freezing point of water (273K), a phase transition between liquid and solid occurs. Therefore, although solid ice and liquid water at close to 273K may be nearly identical in kinetic temperature, the spectral polarization signatures are different.

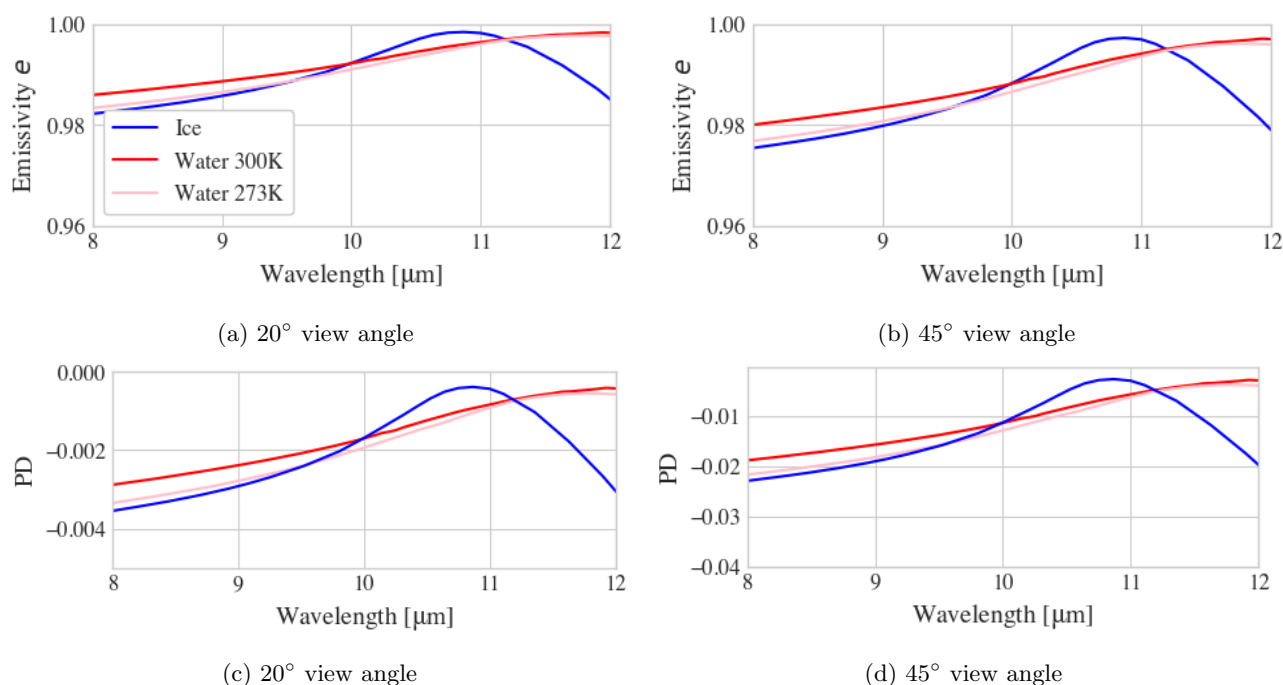


Figure 3: Polarized emissivity in (a) and (b) described as  $\frac{e_p + e_s}{2}$ . In (a) the emissivity of all three samples at 20° view angle is higher compared to (b) 45°. The polarization difference (PD) of the emitted radiance in (c) and (d) is described as  $\frac{e_s - e_p}{e_s + e_p}$ .<sup>21</sup> Polarization magnitude increases from 20° view angle shown in (c) to 45° view angle shown in (d).<sup>17</sup> The emissivity and polarization magnitude of water depend on the kinetic temperature. The emissivity and polarization of ice and water at 300K intersect at approximately 10.0 $\mu$ m and 11.2 $\mu$ m. The emissivity and polarization of ice and water at 273K intersect at approximately 9.5 $\mu$ m and 11.2 $\mu$ m.

## 2. METHODS

### 2.1 Polarimeter

An Infrared Channeled Spectro-Polarimeter (IRCSP) was used to measure ice and water at different viewing angles. The IRCSP measures the linear Stokes parameters with 1K polarimetric accuracy and a spectral resolution of  $1 \mu\text{m}$  on average between 8-12  $\mu\text{m}$ .<sup>1-3,22</sup> The IRCSP uses a quarter-wave retarder followed by a CdSe high-order retarder (HOR) to rotate the incoming polarization as a function of wavelength. The rotated light is then separated into two channels by a wire-grid linear polarizer. A diffraction grating in each path creates a polarization-modulated spectrum which is then imaged with synchronized FLIR Boson microbolometers. The modulation function is

$$M(\lambda, q, u) = q \sin(2\pi\nu\delta_\lambda) + u \cos(2\pi\nu\delta_\lambda). \quad (1)$$

where  $\nu$  is the wavenumber,  $\delta_\lambda$  is the HOR retardance as a function of wavelength, and  $q$  and  $u$  are the normalized Stokes parameters. The amplitude of the modulation function is limited by the polarimetric efficiency, denoted as  $W_{\lambda,\theta}$ , which peaks at 0.6 for the IRCSP. Calibration steps and characterization of the IRCSP is published in prior work.<sup>2,3,22,23</sup>

### 2.2 Data Reduction

The period of the IRCSP modulation function for a given center wavelength  $\lambda_c$  is the spectral window, denoted  $\Delta\lambda$ . The amplitude and phase of modulation is fit within  $\Delta\lambda$ . The average spectral resolution of the instrument is  $1 \mu\text{m}$ , but the size of the spectral window is different for each center wavelength. At  $\lambda_c = 10.6\mu\text{m}$ , the window is 9.9-11.2 $\mu\text{m}$ . In general, the size of the spectral window increases with wavelength.<sup>2,17</sup>

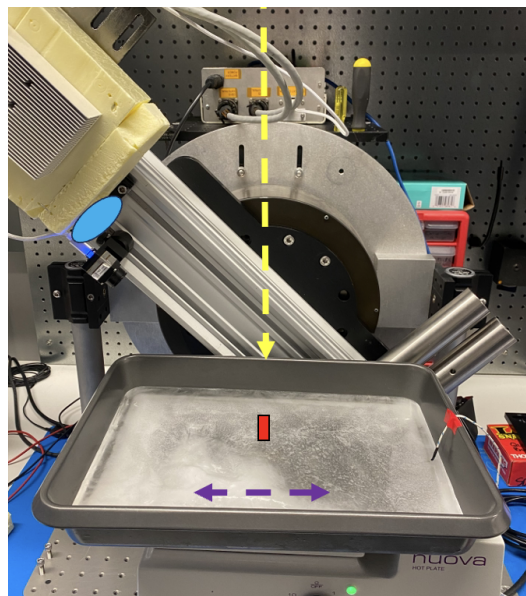


Figure 4: The yellow dashed line indicates a  $0^\circ$  view angle. The aperture is denoted by a blue circle. The spatial HFOV of IRCSP is  $0.36^\circ$  and a red rectangular indicates a 2.54 mm footprint on the sample. The purple line indicates the spectral dimension of the IRCSP.

The Lomb-Scargle Periodogram (LSP) is a widely utilized statistical testing algorithm within the astronomy community. Its purpose is to detect and characterize periodic patterns within unevenly sampled data sets.<sup>24</sup> The modulation function of the IRCSP is unevenly sampled in wavenumber, making the LSP algorithm ideal for demodulation.<sup>22</sup> The retardance is quantified at each wavelength during calibration. If this retardance is identified by the LSP algorithm, an estimate of the coefficients of the following expression is provided.

$$\hat{a} \cos(2\pi\nu\delta_\lambda) + \hat{b} \sin(2\pi\nu\delta_\lambda) \quad (2)$$

Here,  $\hat{a}$  and  $\hat{b}$  are the LSP-estimated weights for a periodic signal of frequency  $\delta_\lambda$ .<sup>25</sup> The normalized Stokes parameters are estimated by including the polarimetric efficiency as the scale factor,  $\hat{u} = \hat{a}/W_{\lambda,\theta}$  and  $\hat{q} = \hat{b}/W_{\lambda,\theta}$ . An open-source LSP Python package *astropy* was used for this computation.<sup>25</sup> These Stokes parameter estimates are used to compute

$$\text{DoLP} = \sqrt{q^2 + u^2}, \quad \text{AoLP} = \frac{1}{2} \tan^{-1} \left( \frac{u}{q} \right). \quad (3)$$

These are the definitions of the degree and angle of linear polarization (DoLP/AoLP).<sup>18</sup> The brightness temperature ( $T_b$ ) is computed using a calibration look-up table of camera counts versus black-body temperature. The IRCSP is capable of retrieving  $T_b$  values within a 1.5K uncertainty.<sup>22</sup>

### 2.3 Measurement Procedures

The experimental setup is shown in Figure 4 where the IRCSP is insulated to control focal plane temperature stability and mounted on the arm of a goniometer. An aluminum 9" × 13" rectangular baking pan was filled with water and frozen overnight with a probe thermistor placed in the water. The pan was positioned at the center of rotation of the goniometer. For repeatability analysis, three consecutive measurements of 10 frames at 60 Hz were taken at each of the following view angles: 0°, ±20°, ±45°. This sequence of three measurements at five angles took six minutes. The temperature of the room during the experiment was 23.5°C.

In the first experiment, the ice was measured in its solid form at 0.4°C, then placed on a hot plate set to 100°C, allowed to melt completely, and measured again once the water came to thermal equilibrium at 34.9°C. During this experiment, the average focal plane temperatures of the cameras were 28.2°C and 27.4°C, with standard deviations of 0.10°C and 0.12°C respectively. The ice was an inch thick and took about an hour to completely melt and warm to thermal equilibrium, so the entire experiment was over a 70 minute time period.

In the second experiment, the ice was measured in its solid form, allowed to melt on the hot plate for 12 minutes until a layer of water formed on the surface, and then the measurement procedure was repeated. The thermistor read 1.5°C for both the solid and melted ice. During this experiment, the average focal plane temperatures of the cameras were 26.7°C and 25.9°C, with standard deviations of 0.09°C and 0.10°C respectively. The duration of the second experiment was 24 minutes.

## 3. RESULTS

Spectrally-resolved IRCSP measurements at 20° view angle are in Figure 5 and view angle dependent results at 10.2 μm are in Figure 6. The error bars are ± one standard deviation from three consecutive measurements.

### 3.1 Variation with Wavelength

Figure 5a are brightness temperature measurements from both experiments to compare ice, melting ice, and water. The  $T_b$  values and error bars of ice and melting ice samples overlap each other. For solid ice and water, the brightness temperature measurements are sufficient for detecting differences. The  $T_b$  values of melted ice at a similar kinetic temperature to solid ice are within one standard deviation of each other. Figure 5b shows the

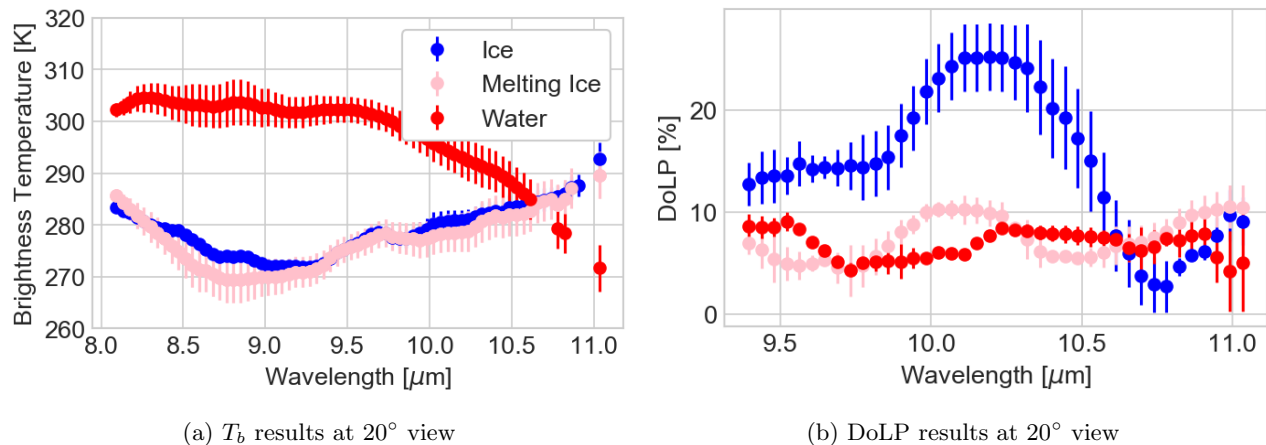
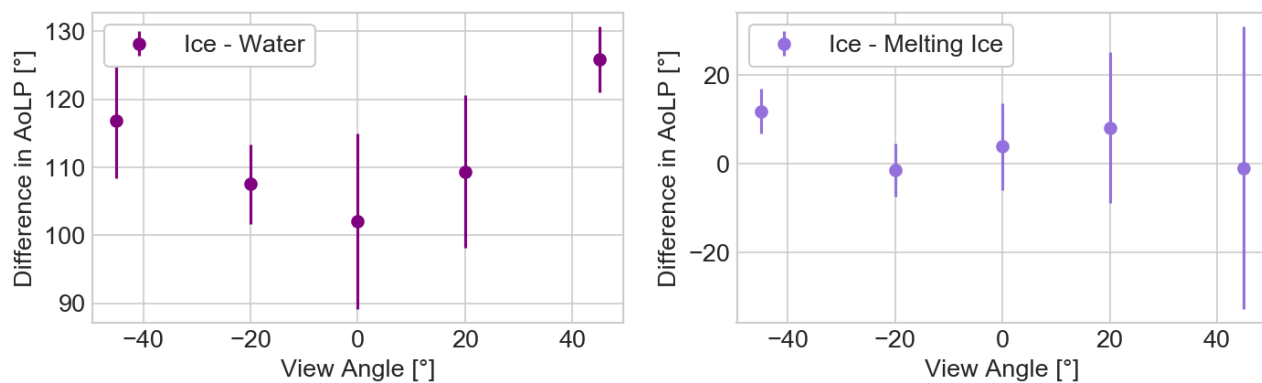


Figure 5: Wavelength-dependent brightness temperature and DoLP results where warm water (red) and melting ice (pink) are compared to solid ice (blue) at the 20° view angle. Ice has resolvable differences in DoLP compared to both the water and melting ice sample, even while the ice and melting ice are the same brightness temperature. The 25% DoLP peak of ice is a feature that is not observed in the water or melting ice. The  $T_b$  and DoLP values for the water, solid ice, and melting ice cross at 10.6 μm. The DoLP values of ice and melting ice intersect again at 11.0 μm

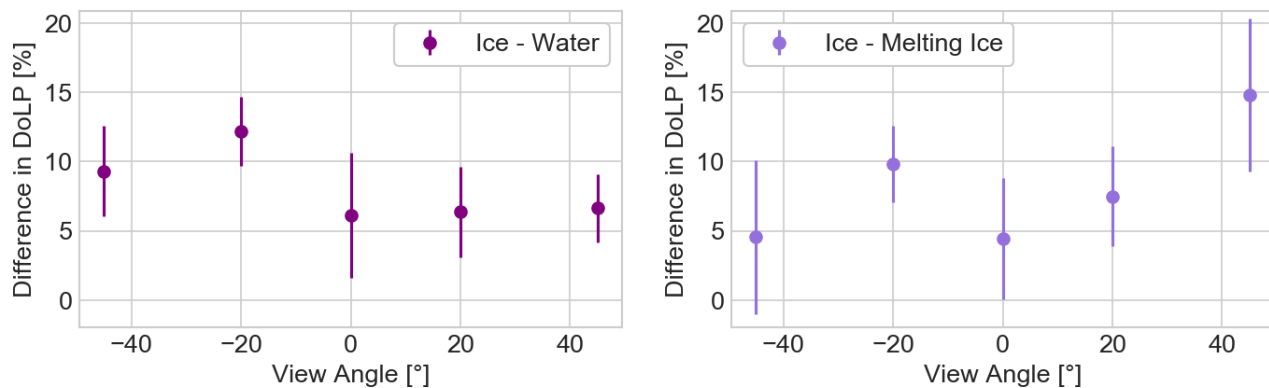
DoLP results of ice compared to melting ice and water. It is notable that the  $T_b$  and DoLP values for the water, solid ice, and melting ice cross at  $10.6\mu\text{m}$ . Recall that in Figure 3, the emissivities and polarization differences of ice and  $300\text{K}$  water crossed around  $10.0\mu\text{m}$ . This equality is within the IRCSP spectral resolution at  $10.6\mu\text{m}$ . The DoLP values of ice and melting ice in Figure 5b intersect again at  $11.0\mu\text{m}$ . Figure 3 also demonstrated an expected crossing point of the polarization of ice and  $273\text{K}$  water at  $11.2\mu\text{m}$ , which is within the spectral window centered around  $11.0\mu\text{m}$ .

Horizontal polarization in the LWIR is associated with a polarization signature dominated by reflection, whereas vertical polarization indicates a signature dominated by emission.<sup>20,26</sup> For an object at thermal equilibrium with its optical background, the polarization signature is equally due to reflection and emission and the two orthogonal states incoherently combine to create unpolarized light. As an object gets closer in temperature to its optical background, the polarization magnitude is expected to decrease.<sup>26</sup> The solid ice is observed to have a higher DoLP than the water sample across most of the spectral range. This is likely due to a greater temperature difference between the ice sample and the ambient environment, whereas the warm water was closer in temperature to the ambient environment. However, the kinetic temperatures of the ice and partially melted ice are similar with respect to their thermal environment. Therefore, observed differences in DoLP are likely dominated by the different indices of refraction for solid ice and water at  $273\text{K}$  shown in Figure 1.



(a) Experiment 1: Difference in AoLP values at  $10.2\mu\text{m}$

(b) Experiment 2: Difference in AoLP values at  $10.2\mu\text{m}$



(c) Experiment 1: Difference in DoLP values at  $10.2\mu\text{m}$

(d) Experiment 2: Difference in DoLP values at  $10.2\mu\text{m}$

Figure 6: The ice-water experiment (dark purple) and ice-melting ice experiment (light purple) are compared by differences in AoLP (a,b) and DoLP in (c,d). The AoLP difference between solid ice and water in (a) is much larger compared to the AoLP difference between ice and melting ice. This trend correlates with the expectation that water is more emissive and therefore p-polarized compared to reflection dominated s-polarization from samples colder than the thermal environment. DoLP results in (c) and (d) show that at every angle, solid ice had a higher DoLP (positive difference) compared to both melting ice and water.

### 3.2 Variation with View Angle

As discussed above, objects that are emitting are expected to be vertically polarized and objects that are reflecting are expected to be horizontally polarized.<sup>26</sup> This expectation is shown in Figures 6a and 6b. In the first experiment, the difference in the AoLP retrievals of warm water and solid ice is around 110°. This AoLP difference indicates that the warm water predominately p-polarized due to emission and the ice radiation is predominately s-polarized due to reflection of the thermal environment. In the second experiment, where the two samples were ice and partially melted ice, the difference in AoLP retrievals was near zero. This correctly indicates that both samples were reflecting radiation and were close in temperature.

### 3.3 Conclusion

The refractive index differences of water and ice are expected to create differences in their spectral LWIR polarimetric signatures. In this work, an Infrared Channeled Spectro-Polarimeter (IRCSP) with an average 1 $\mu$ m spectral resolution measured water, melting ice, and solid ice at room temperature over varying view angles. Repeatable differences in the spectrally dependent DoLP of ice and partially melted ice were observed in the 9.5-10.5 $\mu$ m waveband where on average the DoLP difference was 7% with a peak at 13%. The IRCSP brightness temperature measurements were indistinguishable for these samples. An equality of the brightness temperatures and DoLPs of ice, melted ice, and water were observed at 10.6 $\mu$ m. The spectral emissivity and modeled polarization difference of these samples intersect at approximately 10.0 $\mu$ m, which is within the IRCSP spectral resolution of the 10.6 $\mu$ m measurement equality. These results show that spectrally-resolved LWIR polarimetry can observe both equalities and differences for thermodynamic phase of water depending upon the selected waveband. These LWIR polarimetric features could be used as optical markers for challenging ice-water discrimination tasks in uncontrolled thermal environments.

## REFERENCES

- [1] Hart, K. A., Chipman, R. A., and Wu, D. L., "Compact LWIR polarimeter for cirrus ice properties," *Polarization: Measurement, Analysis, and Remote Sensing XIII* **10655**, 106550V (2018).
- [2] Hart, K. A., Kupinski, M. K., Wu, D. L., and Chipman, R. A., "First results from an uncooled LWIR polarimeter for cubesat deployment," *Optical Engineering* **59**(7), 075103 (2020).
- [3] Shanks, K. A., Chipman, R. A., John, J. A., and Kupinski, M. K., "Near space demonstration of a compact LWIR spectro-polarimeter for ice cloud measurements," *Polarization: Measurement, Analysis, and Remote Sensing XV* **12112**, 143 – 159 (2022).
- [4] NASA, "IceSAT-: Ice, cloud, and land elevation satellite." <https://icesat-2.gsfc.nasa.gov/mission> (2018).
- [5] Kwok, R., G.F. C., J., H., and T., M., "Testing the ice-water discrimination and freeboard retrieval algorithms for the icesat-2 mission," *Remote Sensing of Environment* **183**, 13–25 (2016).
- [6] Nekrasov, A., Khachaturian, A., Abramov, E., Kurdel, P., Gamcová, M., Gamec, J., and Bogachev, M., "On sea ice/water discrimination by airborne weather radar," *IEEE Access* **8**, 120916–120922 (2020).
- [7] Melsheimer, C., Spreen, G., Ye, Y., and Shokr, M., "First results of antarctic sea ice type retrieval from active and passive microwave remote sensing data," *The Cryosphere* **17**(1), 105–126 (2023).
- [8] Gong, J. and Wu, D. L., "Microphysical properties of frozen particles inferred from Global Precipitation Measurement (GPM) Microwave Imager (GMI) polarimetric measurements," *Atmospheric Chemistry and Physics* **17**(4), 2741–2757 (2017).
- [9] Gong, J., Zeng, X., Wu, D. L., and Li, X., "Diurnal variation of tropical ice cloud microphysics: Evidence from global precipitation measurement microwave imager polarimetric measurements," *Geophysical Research Letters* **45**(2), 1185–1193 (2017).
- [10] Lewis, J. R., Campbell, J. R., Stewart, S. A., Tan, I., Welton, E. J., and Lolli, S., "Determining cloud thermodynamic phase from the polarized micro pulse lidar," *Atmospheric Measurement Techniques* **13**, 6901–6913 (2020).
- [11] Pilewskie, P. and S., T., "Discrimination of ice from water in clouds by optical remote sensing," *Atmospheric Research* **21**, 112–122 (1987).

- [12] Abdelaal, A., Sarayloo, M., Nims, D. K., Mohammadian, B., Heil, J., and Sojoudi, H., “A flexible surface-mountable sensor for ice detection and non-destructive measurement of liquid water content in snow,” *Cold Regions Science and Technology* **195** (2022).
- [13] Polyanskiy, M. N., “Refractive index database.” <https://refractiveindex.info> (2008).
- [14] Bohren, C. F. and Huffman, D. R., [*Absorption and scattering of light by small particles*], John Wiley & Sons (2008).
- [15] Hapke, B., [*Theory of Reflectance and Emittance Spectroscopy*], Cambridge University Press (1993).
- [16] Hancer, M., Sperline, R. P., and Miller, J. D., “Anomalous dispersion effects in the IR-ATR spectroscopy of water,” *Applied Spectroscopy* **54**, 1–158 (2020).
- [17] Shanks, K. A., *Infrared Polarimetry for Remote Sensing*, PhD thesis, University of Arizona (2022).
- [18] Chipman, R. A., Lam, W. S. T., and Young, G., [*Polarized light and optical systems*], CRC Press (2018).
- [19] Hagen, N., “Review of thermal infrared polarimetry, i: theory,” *Optical Engineering* **61**(7), 070902 (2022).
- [20] Shaw, J. A., “Degree of linear polarization in spectral radiance from water-viewing infrared radiometers,” *Appl. Opt.* **38**, 3157–3165 (1999).
- [21] Shaw, Joseph A. and Marston, C., “Polarized infrared emissivity for a rough water surface,” *Appl. Opt.* **7**, 375–380 (2000).
- [22] Shanks, K. A., John, J. A., Parkinson, J. C., Wu, D. L., and Kupinski, M. K., “High-altitude demonstration of LWIR polarimeter using uncooled microbolometer,” *Journal of Quantitative Spectroscopy and Radiative Transfer (JQSRT) (in review)* (2023).
- [23] Hart, K. A., Wu, D. L., Chipman, R. A., and Kupinski, M. K. K., “Stokes resolved differential temperature: an important metric of polarimetric precision in the long-wave infrared,” (2021).
- [24] Lomb, N. R., “Least-squares frequency analysis of unequally spaced data,” *Astrophysics and space science* **39**(2), 447–462 (1976).
- [25] astropy.timeseries, “Lomb-scargle periodograms.” <https://docs.astropy.org/en/stable/timeseries/lombscargle.html> (2011).
- [26] Tyo, J. S., Ratliff, B. M., Boger, J. K., Black, W. T., Bowers, D. L., and Fetrow, M. P., “The effects of thermal equilibrium and contrast in LWIR polarimetric images.” <https://opg.optica.org/oe/fulltext.cfm?uri=oe-15-23-15161&id=144634> ((2007)).